Higher-order nonlinear modes and bifurcation phenomena due to degenerate parametric four-wave mixing

Kazimir Y. Kolossovski, Alexander V. Buryak, and Victoria V. Steblina
School of Mathematics and Statistics, University College, Australian Defence Force Academy, Canberra 2600, Australia

Alan R. Champneys
Department of Engineering Mathematics, University of Bristol, Bristol BS8 1TR, United Kingdom

Rowland A. Sammut
School of Mathematics and Statistics, University College, Australian Defence Force Academy, Canberra 2600, Australia
(Received 7 March 2000)

We demonstrate that weak parametric interaction of a fundamental beam with its third harmonic field in Kerr media gives rise to a rich variety of families of nonfundamental (multihumped) solitary waves. Making a comprehensive comparison between bifurcation phenomena for these families in bulk media and planar waveguides, we discover two types of soliton bifurcations and other interesting findings. The latter includes (i) multihumped solitary waves without even or odd symmetry and (ii) multihumped solitary waves with large separation between their humps which, however, may not be viewed as bound states of several distinct one-humped solitons.

PACS number(s): 42.65.Tg, 05.45.Yv, 42.65.Ky

I. INTRODUCTION AND MODEL

Recently, parametric wave mixing in Kerr media has attracted significant attention (see, e.g., Refs. [1–3] where continuous-wave interaction and parametric self trapping were investigated). This theoretical activity has been backed up by experimental advances, e.g., a scheme for quasiphase matched third-harmonic generation (THG) has been suggested [4]. However, in previous works devoted to spatial solitary waves due to THG in planar waveguides, only families of fundamental self-trapped beams were considered. In Ref. [3], for example, where solitons due to third-harmonic generation were considered for a bulk medium geometry, higher-order modes were not discussed in detail. By soliton we mean a localized mode. By *higher-order* we refer to beam shapes whose transverse intensity typically has a multipeaked structure and has higher energy than the single-peaked fundamental state.

Physically stationary states define the distribution of the fields between harmonics of self-trapped beams at a given value of the total power. Such stable stationary solitons may appear as final states of beam evolution. Unstable stationary solitons also play an important role in determining the initial beam evolution (see, e.g., Ref. [5]) providing a rich variety of possible instability development scenarios and sometimes being attractors for intermediate beam evolution stages. Hence, the knowledge of the set of all possible stationary-soliton states and their stability gives a rough answer to the question: *what type of output beams can we expect for a given initial input beam?* The complete information about the existence and stability of higher-order soliton modes may also be important for the design of all-optical devices with sharp switching characteristics (see Ref. [6] for an example).

This paper concerns the first step in such a complete investigation of all possible localized modes of the THG model, namely the existence, but not stability, of higher-order states. Specifically, we analyze in full detail the structure and bifurcation phenomena of higher-order bright spatially localized modes. The spatial configuration is assumed to be such that there is a well-defined propagation direction and the beams are localized in n transverse directions, with $n=1$ representing a planar waveguide and $n=2$ a bulk medium. Specifically we study models representing (1+1)-dimensional [(1+1)D] and (2+1)-dimensional [(2+1)D], weakly anisotropic media with cubic nonlinearity, under the phase-matched condition that the fundamental wave is resonantly coupled to its third harmonic. This is a particular degenerate case of solitons supported by the four-wave mixing processes [7], which is not completely understood yet in full generality. We assume that the interaction between the fundamental and third-harmonic waves includes the effects of parametric four-wave mixing, self-phase modulation, and cross-phase modulation.

We closely follow the derivation procedure of Ref. [2], assuming that the fundamental and the third-harmonic beams have the same linear polarization. The result is the following normalized (dimensionless) system of coupled equations

$$i\frac{\partial u}{\partial z}+\nabla^2 u-u+\left(\frac{1}{9}|u|^2+2|w|^2\right)u+\frac{1}{3}u^{*2}w=0,$$

$$i\sigma\frac{\partial w}{\partial z}+\nabla^2 w-\alpha w+(9|w|^2+2|u|^2)w+\frac{1}{9}u^3=0, \quad (1)$$

where u and w are the fundamental and third harmonics, respectively. Also for the case of spatial beams $\nabla^2\equiv\partial^2/\partial x^2+\partial^2/\partial y^2$ in the (2+1)-dimensional case, or $\nabla^2\equiv\partial^2/\partial x^2$ in the (1+1)D case. The parameter α measures the shift in the propagation constant, which is induced by the nonlinearity and is also dependent on the quality of wave-vector matching

1063-651X/2000/62(3)/4309(9)/$15.00

between the harmonics, with $\alpha=3\sigma$ corresponding to exact matching, and z is the propagation distance. For the spatial soliton case, the dimensionless parameter σ is the ratio of the wave numbers of the harmonics and is equal to 3. Note that the system (1) may also describe temporal pulse propagation of resonantly interacting fundamental and third harmonics in optical fibers. For this physical situation $\nabla^2\equiv\partial^2/\partial t^2$ (t is the retarded time variable) and σ is the absolute value of the ratio of second-order group velocity dispersions for the first and the third harmonics and may be any positive number.

Radially symmetric stationary beams are described by real solutions, $u(r)$ and $w(r)$ that are defined by the system

$$\frac{d^2u}{dr^2}+\frac{s}{r}\frac{du}{dr}-u+\left(\frac{1}{9}u^2+2w^2\right)u+\frac{1}{3}u^2w=0,$$

$$\frac{d^2w}{dr^2}+\frac{s}{r}\frac{dw}{dr}-\alpha w+(9w^2+2u^2)w+\frac{1}{9}u^3=0. \tag{2}$$

Here $r\equiv\sqrt{x^2+y^2}$ and $s=1$ for the (2+1)D case, whereas $r\equiv x$ and $s=0$ for the (1+1)D case. These localized solutions depend only on a single dimensionless parameter α. Analysis of the linear part of Eqs. (2) in the limit $r\rightarrow\infty$ shows that conventional bright solitons (with exponentially decaying tails) can exist only for $\alpha>0$.

By ''bright symmetric'' in the remainder of this paper we shall mean (2+1)D solutions when the intensity of each localized harmonic reaches a maximum at $r=0$ and (1+1)D solutions with $u(r)=u(-r)$ and $w(r)=w(-r)$. Thus, we shall only seek these solutions on the interval $0\leqslant r\leqslant\infty$ even in the $(1+1)$D case. Note further that Eqs. (2) have odd symmetry, that is, if $[u(r),w(r)]$ is a solution then so is $[-u(r),-w(r)]$. Thus all solutions must come in pairs, the second solution being simply a change in sign (a phase shift of π) of both harmonics. For the case $s=0$, it is additionally possible to have solutions that are odd in both harmonics, or which are neither odd nor even. The latter type of solutions we shall refer to as being ''bright asymmetric.'' In this paper, we shall consider mainly the solitons of bright symmetric type, but shall also present some results about bright asymmetric (1+1)D solitons. Dark solitons (localized solutions with nonzero asymptotics) are out of the scope of this paper.

The case $\alpha<0$ also has physical meaning, but there one should expect to find *quasisolitons*, which are almost localized stationary states that have small periodic oscillations in their tails. See, e.g., [3,8–10] for the definition, examples and for some issues surrounding them. Quasisolitons in this model will form the subject of another work. Here we shall concentrate almost exclusively on the case $\alpha>0$.

Using a direct analogy with the theory of $\chi^{(2)}$ (second-harmonic generation) solitons (e.g., Ref. [11]), we start our analysis from the so-called cascading limit when $\alpha\gg1$. In this limit $w\approx u^3/(9\alpha)$ and the equation for u approaches the cubic-quintic nonlinear Schrödinger (NLS) equation. This scalar equation possesses a familiar class of fundamental bright solitons consisting of a simple bell-shape [there are also higher-order families in the (2+1)D case]. These fundamental solitons can then be used as a starting point in the search for families of stationary solutions using numerical

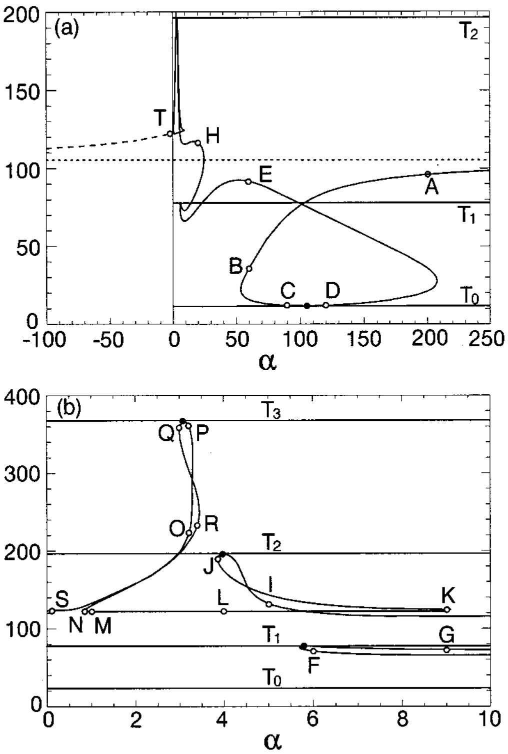

FIG. 1. (a) Bifurcation diagram for solitons (solid curves) and quasisolitons (dashed curves) of Eqs. (1) in the (2+1)D case. (b) Expanded portion of (a) for the range $0\leqslant\alpha\leqslant10$. Examples of solitons are shown in Figs. 2–7. Bifurcation points of two-wave solitons from one-wave soliton families are shown by filled circles. The results related to quasisolitons are for stationary solutions with *minimal* amplitude of oscillatory tails; in that case, P is calculated for the soliton core only. In this and all subsequent figures, units are dimensionless.

methods. These methods comprise a standard shooting method at fixed α, and a continuation method allied to solution using a relaxation method for solving an appropriately defined two-point boundary-value problem for Eqs. (2). This latter technique can trace paths of solutions as α varies. We choose to characterize these solitons by the value of normalized total power that is one of the conserved quantities of the system (1)

$$P_{\rm tot}=\int_A(|u|^2+3\sigma|w|^2)dA. \tag{3}$$

Here the integration extends over the appropriate one- or two-dimensional infinite cross-section A.

The dependence of $P_{\rm tot}$ on α for a branch of solitons is usually, at least in the case of a fundamental solution, closely related to its stability. A necessary condition for stability in the case of fundamental multicomponent solitons is typically given by a generalized Vakhitov-Kolokolov (VK) criterion [12], which often also appears to be a sufficient condition for soliton stability (see, e.g., Refs. [13]). However, the complexity of Eqs. (1) which, for example, possess collapse-type dynamics in the (2+1)D case, may lead to instability of fundamental solitons even for branches that are supposed to be stable according to the VK criterion [3]. Thus, below we use

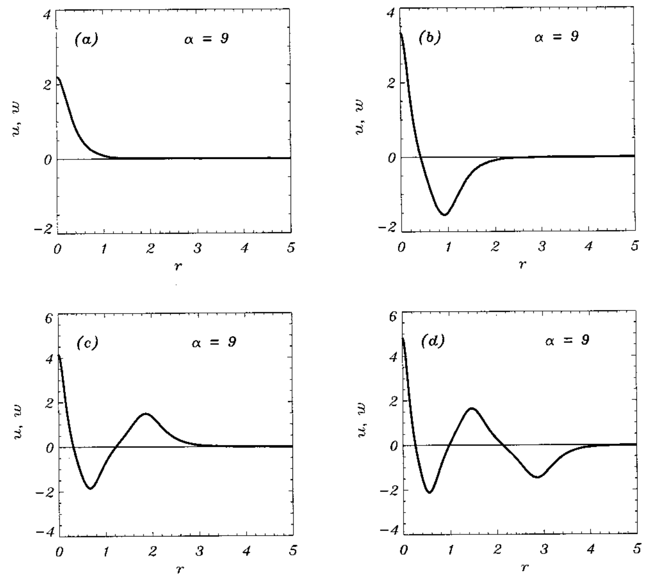

FIG. 2. Examples of different families of one wave solitons. In all diagrams, the thick line corresponds to the third harmonic.

power versus-α dependence only for classification of soliton families, leaving a full-scale stability analysis for future consideration.

II. RESULTS FOR BULK MEDIA

First we present the results for the (2+1)D case. Figure 1 shows the variation of the normalized total power $P_{\rm tot}$, with the normalized mismatch parameter α, for different types of one-wave and two-wave localized solutions of the system (1) with $s=1$. The corresponding soliton profiles at various points along the presented branches are given in Figs. 2–7.

The first class of localized solutions of the system (1) consists of one-frequency soliton families for the third harmonic w_0, which exist for all $\alpha>0$ and represent scalar Kerr solitons described by the standard cubic NLS equation that

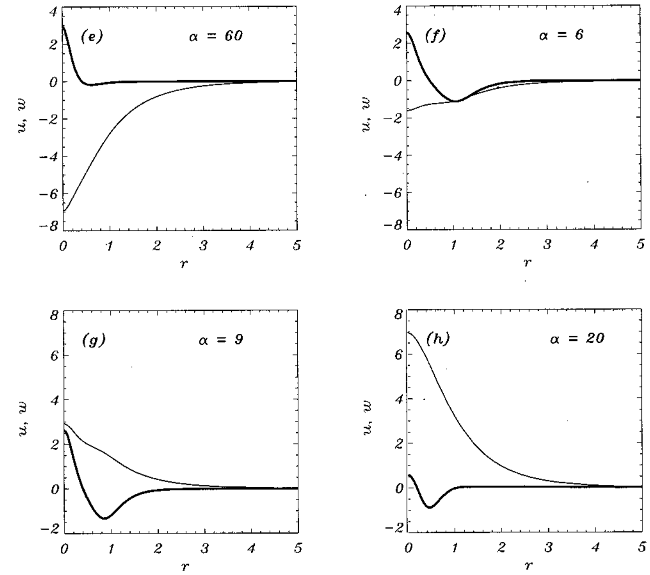

FIG. 4. Examples of (2+1)D two-wave solitons. Labeling of examples corresponds to labeling of open circles in Fig. 1.

follows from the second of Eqs. (1) at $u=0$:

$$\frac{d^2 w_0}{dr^2}+\frac{1}{r}\,\frac{dw_0}{dr}-\alpha w_0+9w_0^3=0. \tag{4}$$

These single-frequency solitons differ from each other by the number of zero crossings in their radial profiles so that we denote the corresponding families as T_0 (no crossing), T_1 (one crossing), T_2 (two crossings), etc. Examples of one-wave solitons belonging to different T_j families are shown in Fig. 2. Note that the normalized power $P_{\rm tot}$ is constant for each of the T_i families. For example, for the fundamental one-wave soliton family T_0 (which are, in fact, Townes solitons of Ref. [14]) we have $P_{\rm tot}\approx 11.70$ for all $\alpha>0$.

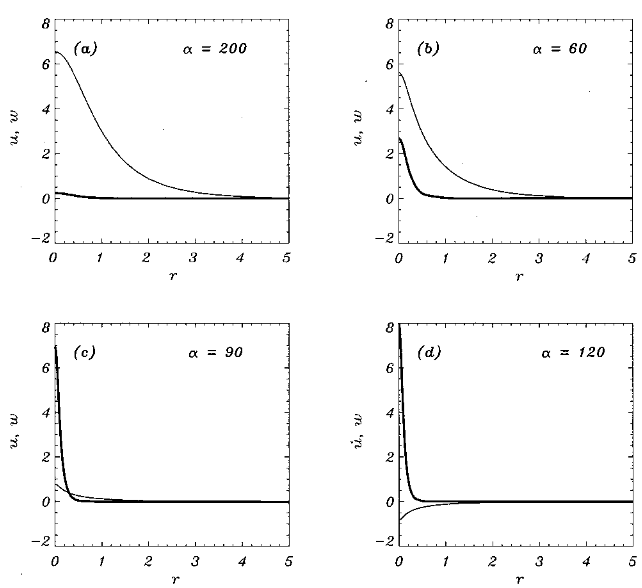

FIG. 3. Examples of (2+1)D two-wave solitons. Labeling of examples corresponds to labeling of open circles in Fig. 1.

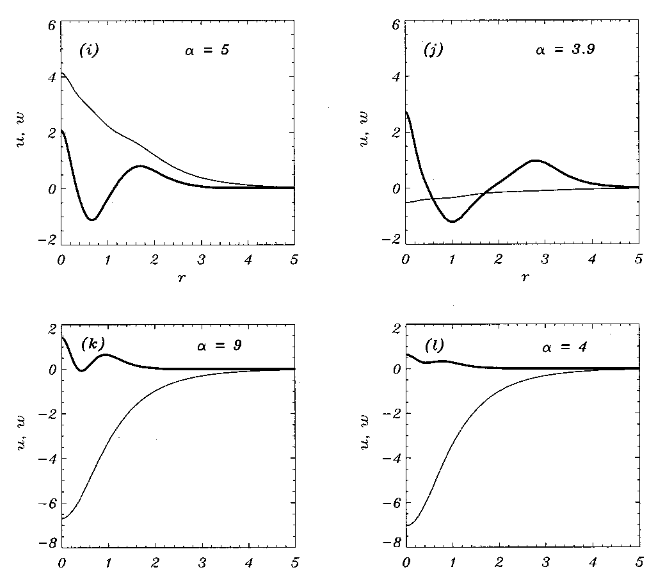

FIG. 5. Examples of (2+1)D two-wave solitons. Labeling of examples corresponds to labeling of open circles in Fig. 1.

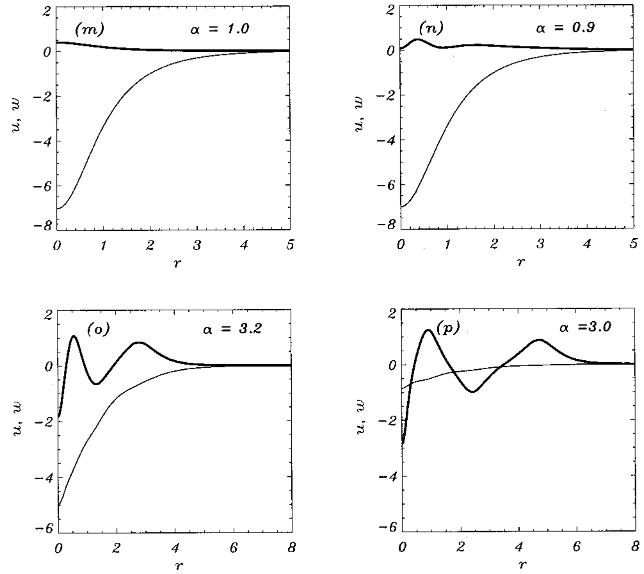

FIG. 6. Examples of (2+1)D two-wave solitons. Labeling of examples corresponds to labeling of open circles in Fig. 1.

The second class of solutions to Eqs. (1) are genuinely two-wave bright solitons, described by families of localized beams with coupled fundamental and third harmonics. The simplest way to obtain such solutions numerically is to follow the two-wave soliton families from the cascading limit (large α) as α decreases. In this work, we concentrate on the result of following the lowest order two-wave soliton branch whose profiles have a simple one-hump form in the cascading limit. For this family, painstaking numerical continuation reveals a highly complex solution path involving restructuring of the soliton profile while the corresponding $P(\alpha)$ curve undergoes several loops (see Figs. 1 and 8). Inherent in each loop is a touch with one of the T_i families. Such a touch corresponds to a transcritical bifurcation from the pure w solution, and note [for example, from Figs. 3(c),(d) that correspond to points C and D on Fig. 1(a)] that the two different bifurcating branches have opposite signs of their u component. The fact that these bifurcations take place further illustrates the severity of the restructuring of the soliton profiles that must take place; in the cascading limit the branch is approximately of pure u type, whereas at each bifurcation with T_i it is composed of purely a third-harmonic component w. Figures 2–7 illustrate the complete restructuring process by depicting the soliton profiles in the vicinity of each bifurcation and turning point of the $P(\alpha)$ curve. Note finally that the two-wave soliton family also includes the simplest so-called self-similar [for which $u(r)\propto w(r)$] solution (Fig. 1, point M) at $\alpha=1$, see Ref. [15] for the details and also Ref. [2], where its (1+1)-dimensional counterpart was also been considered.

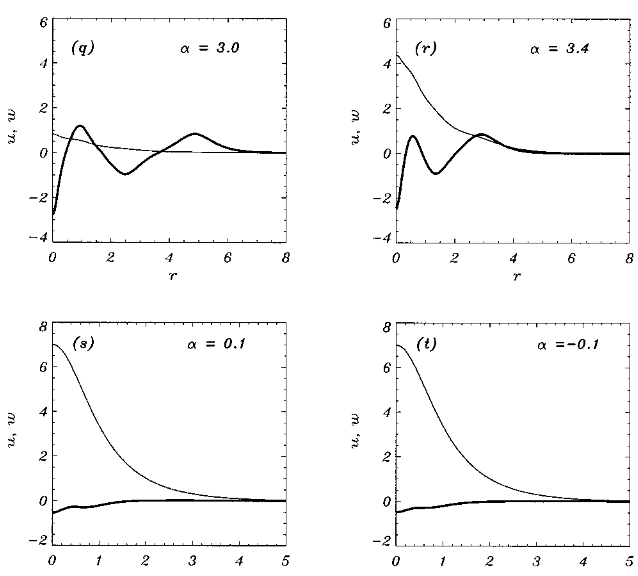

FIG. 7. Examples of (2+1)D two-wave solitons and quasisolitons. Labeling of examples corresponds to labeling of open circles in Fig. 1.

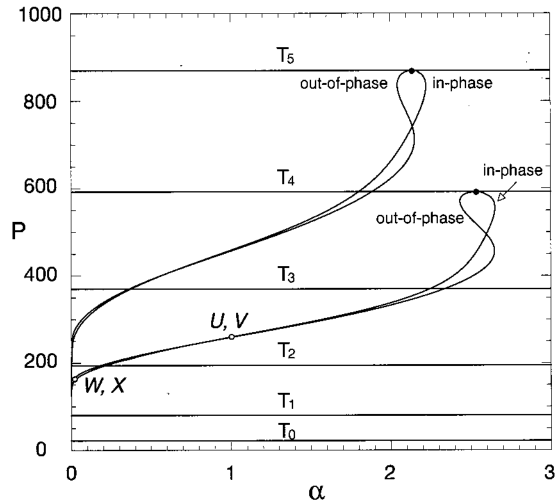

FIG. 8. Bifurcation diagram from higher-order families, T_i, $i>3$.

The position of the bifurcation point from the T_0 branch can be approximately calculated analytically. Linearization of Eqs. (1) around the solution $w_0(r)$ gives the eigenvalue equation

$$\frac{d^2u_1}{dr^2}+\frac{1}{r}\frac{du_1}{dr}+2w_0^2(r)u_1=\lambda u_1, \tag{5}$$

together with appropriate boundary conditions. Bifurcations occur when $\lambda=1$. This may also be viewed as the problem of existence of localized states in the potential $U(r)=-2w_0^2(r)$ with eigenvalue λ. Due to the lack of a closed form analytical expression for $w_0^2(r)$, solutions of Eq. (5) may be approximated by feeding in the numerical data for w_0 or by analytical techniques based on a variational approximation. Using the latter, based on a simple exponential trial function, gives the result $w_0=\sqrt{8\alpha}/3e^{-r\sqrt{\alpha}}$. Substituting this into Eq. (5) and assuming a similar form of trial function for u_1, one can use a Rayleigh-Ritz method to obtain $\alpha_{bif}^{(var)}=105.8$. This agrees to within 2% with the numerical result $\alpha_{bif}^{(num)}=104.2$. Calculation of bifurcation points along the higher-order T_i branches may in principle be carried out by the same method. However, this is less straightforward technically because it requires the use of complicated forms

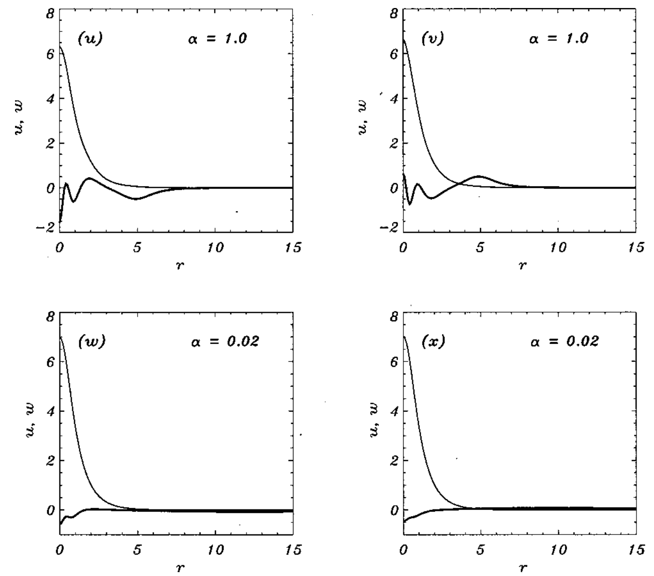

FIG. 9. Spreading of the solutions bifurcated from the T_4 in the limit $\alpha\rightarrow 0$; (u,w) ''out-of-phase'' solitons, (v,x) ''inphase'' solitons. Labeling of the profiles is in agreement with labeling in Fig. 8.

of trial functions, and it is perhaps more instructive to rely on numerical detection of the bifurcation points. Symmetry arguments dictate that at each bifurcation point α_{bif} there will exist two different bifurcating solutions of Eq. (5): $u_1(r)$ and $-u_1(r)$. Moreover, each bifurcation is a transcritical and gives rise to a pair of two-wave branches $[w_0(r), \pm\varepsilon u_1(r)]$, where ε is proportional to $|\alpha-\alpha_{bif}|$.

The third class of solutions to Eqs. (1) are the aforementioned quasisolitons that exist in the region of negative α. We do not discuss quasisolitons here in any detail. A full analysis will appear elsewhere. We simply make the comment that the branch SOP bifurcating from T_3 can be continued up to the boundary $\alpha=0$ separating regular from quasisolitons. On the other side of the boundary a similar quasisoliton state can be found with tiny oscillations in its tail [see Figs. 1 and 7(t,s)].

We note that there are also higher-order two-wave soliton families that are not linked to the cascading limit solitons. These families bifurcate from the T_i $(i\geqslant 4)$ families. Each of these bifurcating branches can be continued smoothly up to $\alpha=0$ like the family SOP. Figure 8 shows the branches from the next two one-frequency solutions T_4 and T_5. We conjecture that each T_i branch for $i>3$ also exhibits a unique bifurcation point, with the α-values of the bifurcation point tending to zero as $i\rightarrow\infty$. Initially the two branches bifurcated from each T_i have the opposite phase of the third-harmonic component. Figure 9 shows the soliton profiles of the ''inphase'' $[u(r=0)w(r=0)>0$ close to the bifurcation] and ''out-of-phase'' $[u(r=0)w(r=0)<0]$ branches that bifurcate from T_4. As $\alpha\rightarrow 0$, the difference between the branches becomes negligible as the third-harmonic of all branches becomes out-of-phase with the fundamental component. Meanwhile the peaks of the third-harmonic broaden and ''spread out'' toward $r=\infty$. Close to $\alpha=0$, solitons of the branches differ only by the fine structure of their wings in the third-harmonic component [see Figs. 7(s,t) and Figs. 9(c,d)].

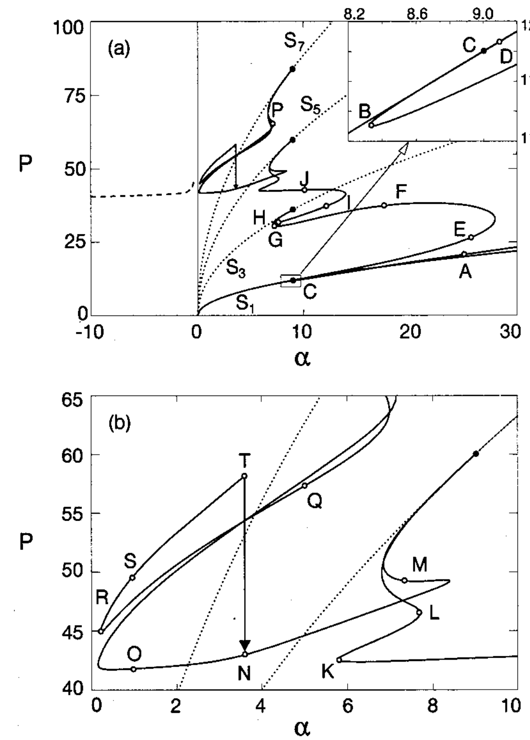

FIG. 10. (a) Bifurcation diagram for symmetric solitons (solid curves) and quasisolitons (dashed curve) of the (1+1)D version of Eqs. (1). (b) Expanded portion of (a) in the range $0\leqslant\alpha\leqslant 10$, $40\leqslant P\leqslant 65$. Dotted curves emerging at zero correspond to integer multiples of the primary one-wave solution S_1. Formally they represent multisoliton states consisting of a concatenation of infinitely separated single solitons. Points at which branches of two-wave solitons terminate by ''bifurcating'' from one of these multisolitons are depicted by filled circles and all occur for $\alpha=9$. The inset to (a) and the jump $(T\rightarrow N)$ depicted in (b) are explained in the text.

III. RESULTS FOR PLANAR WAVEGUIDES

It is interesting to compare the (2+1)D results discussed above with those for the corresponding (1+1)D case. The bifurcation diagram related to the (1+1)D case is presented in Fig. 10 and the corresponding examples of soliton profiles are given in Figs. 11–16. We now highlight how, together with many obvious differences in comparison to the diagram for the (2+1)D case in Fig. 1, there are also some striking similarities as well. Note that in some respects the model for the (1+1)D case is simpler since the corresponding stationary system (2) with $s=0$ does not depend explicitly on r and hence represents an autonomous dynamical system in four dimensions. Finding solitons is then reduced to finding homoclinic trajectories in this 4D phase space.

The first class of (1+1)D localized waves of system (1) consists of one-frequency soliton families for the third harmonic w_0, which exist for all $\alpha>0$ and represent scalar Kerr solitons described by the standard cubic (1+1)D NLS equation that follows from the second of Eqs. (1) at $u=0$:

$$\frac{d^2w_0}{dx^2}-\alpha w_0+9w_0^3=0. \tag{6}$$

It can be readily solved exactly giving the well-known unique single soliton solution

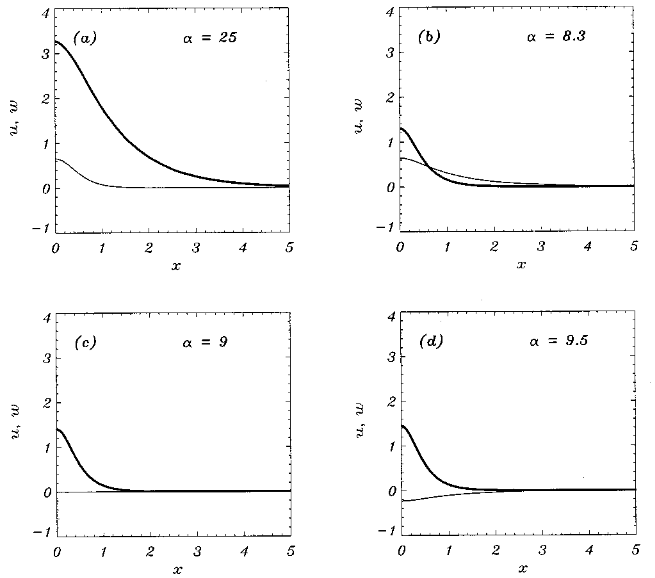

FIG. 11. Examples of (1+1)D two-wave and one-wave solitons. Labeling of all examples corresponds to the labeling of the open circles in Fig. 10.

$$w_0(x)=\frac{\sqrt{2\alpha}}{3}\operatorname{sech}(\sqrt{\alpha}x), \quad P_{\mathrm{tot}}=4\sqrt{\alpha}. \tag{7}$$

In contrast to the (2+1)D case, strictly speaking there are no other one-wave localized solutions. However, it will be helpful in what follows to consider formal multisoliton states consisting of a different number of infinitely separated single solitons (7), families of which we denote by S_1 (single soliton), S_2 (two solitons), S_3 (three solitons), etc. In this work we are mainly interested in families with an odd number of separated solitons: S_{2i+1}, $i=1,2,3,\dots$, but we also investigate ''bifurcations'' from S_2. Note that, for $i>1$, S_i in fact denotes more than a single one-wave family, because each single pulse that is glued together can be either positive or negative.

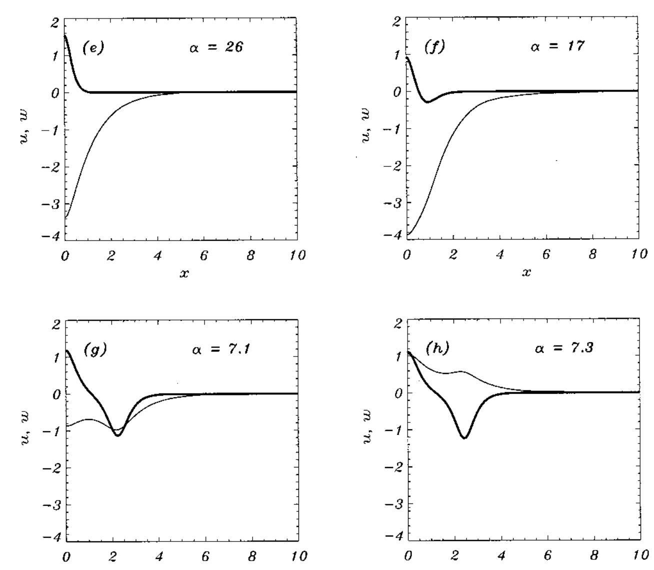

FIG. 12. Examples of (1+1)D two-wave solitons. Labeling is as for Fig. 11.

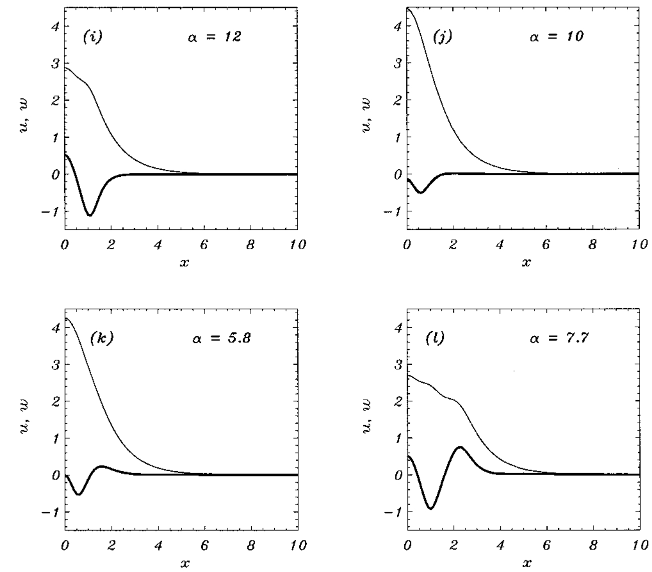

FIG. 13. Examples of (1+1)D two-wave solitons. Labeling is as for Fig. 11.

The second class of (1+1)-dimensional localized solutions of Eqs. (1) consists of two-wave bright symmetric solitons and is described by families of localized beams with coupled fundamental and third harmonics. The simplest way to obtain the lowest order two-wave soliton family is again to continue numerically from solitons of the cascading limit ($\alpha \gg 1$) given approximately by the expression

$$u(x)\approx\frac{6}{\sqrt{1+B\cosh 2x}}, \quad w\approx u^3/(9\alpha), \tag{8}$$

where $B=\sqrt{1+16/\alpha}$. The first expression for $u(x)$ in Eq. (8) is the solution of the corresponding cubic-quintic NLS-type equation.

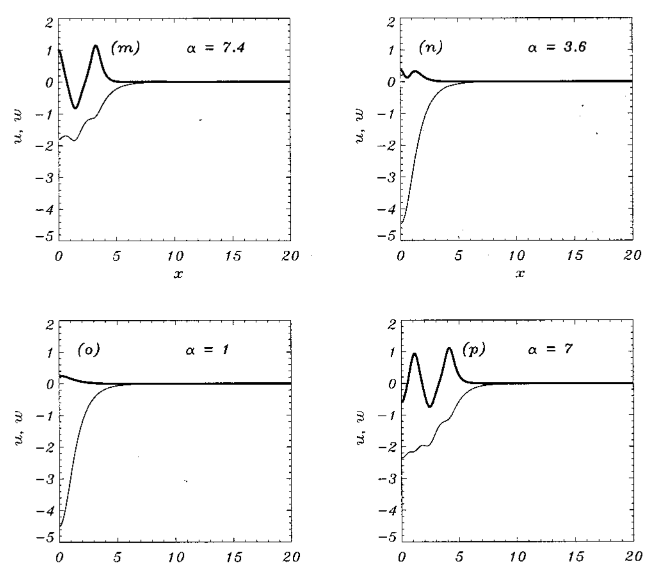

FIG. 14. Examples of (1+1)D two-wave solitons. Labeling is as for Fig. 11.

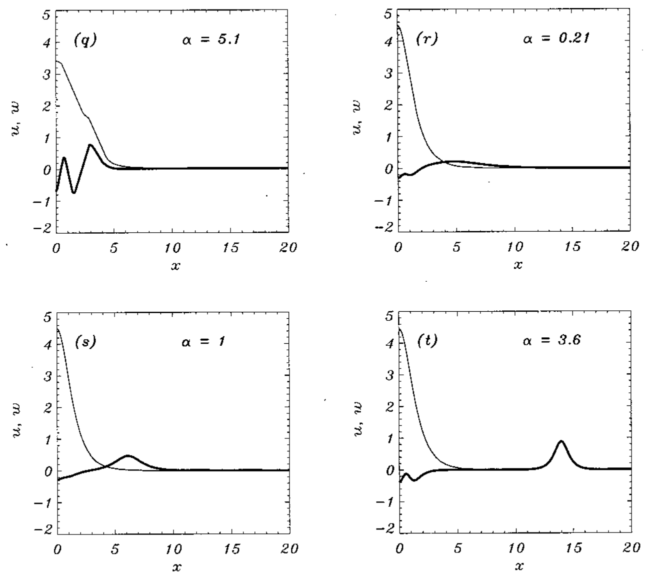

FIG. 15. Examples of (1+1)D two-wave solitons. Labeling is as for Fig. 11.

The results of our numerical continuation from this limiting solution, upon decreasing α is that, like in the (2+1)D case, this branch also traces a convoluted path in the (P,α)-plane, involving four ''bifurcations'' from one-wave soliton families (from the families S_1, S_3, S_5, and S_7). As in the (2+1)D case, this branch connects to a self-similar solution at $\alpha=1$ [the point O in Fig. 10(b)]. In this case, the self-similar solution is expressible in closed analytical form as

$$u(x)=a\,\mathrm{sech}\,x, \quad w(x)=bu(x), \tag{9}$$

where the parameter b is the real root of the cubic equation $63b^3-3b^2+17b+1=0$, and $a^2=18/(18b^2+3b+1)$.

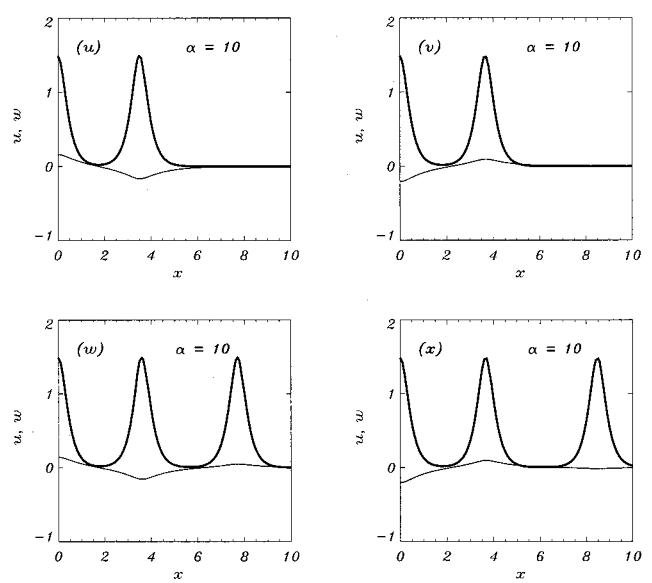

FIG. 16. Examples of (1+1)D two-wave solitons, which are not directly linked to the two-wave solitons of the cascading limit. Labeling is as for Fig. 11.

However, it is here that the similarity with the (2+1)-case ends, as we shall now explain.

First, let us try to motivate what is happening at each of the ''bifurcations'' from S_j; for which at first sight it seems remarkable that each one occurs precisely at $\alpha=9$. Standard bifurcation analysis (e.g., as in Ref. [16]) allows us to find the position of the single bifurcation point from the one-wave soliton family S_1 (7) at $\alpha=9.0$ [point C in Fig. 10(a)]. As in the (2+1)D case, the bifurcation is a transcritical with one branch emerging to the left of the bifurcation point and one to the right. This structure is confirmed by the inset to Fig. 10(a) that shows that the branch emerging to the left undergoes a fold (at point B), so that on a larger scale both branches appear to bifurcate to the right.

Now it seems that this ''local'' bifurcation from S_1 causes a topological change in the four-dimensional phase space so that a global event must also happen at this parameter value. This global event is the possibility of gluing together several copies of the S_1 back to back and forming a new branch of solitons with several large peaks that bifurcate from $\alpha=9$. Phenomenologically this is similar to what happens in the SHG case when the parameter equivalent to α passes through 1 [17,18]. A key observation here is that in order to get a symmetric (even) solution, only an odd number of copies of the S_1 may be taken to form solitons in this way. As a convenient shorthand for this global bifurcation of multi-peaked solutions at $\alpha=9$, we have referred to it as a local ''bifurcation'' from S_{2i+1}, where $i=1,2,3\ldots$, although this is strictly a misnomer.

Numerical continuation beyond point G of Fig. 10(a) shows that the two-wave soliton branch approaches $\alpha=9.0$ from the left, where it bifurcates from the S_3 asymptotic one-wave family that has alternative phase between each single-soliton component. However, we find that this is only one of a total of *four* symmetric two-wave solitons that come out of S_3. There are eight in total if you include the change of sign of both u and w. The second bifurcates to the left from the same (alternating phase) S_3 family and differs only in that the first harmonic has the opposite sign. A representative of this branch, corresponding to point H in Fig. 10(a), is shown in Fig. 12(h). The two other branches exist for $\alpha>9$ and bifurcate from the S_3 family where all peaks are in phase (positive), and representatives are shown in Fig. 16(u,v). With the increase of α (cascading limit) these complex multihumped solitons keep their general structure intact, but become more localized. These two branches are not shown in the bifurcation diagram (Fig. 10) but their $P(\alpha)$ curves lie very close to each other and to the T_3 curve to the right of the bifurcation point.

A similar bifurcation picture is observed at $\alpha=9.0$ for bifurcations from S_5 and S_7 one-wave families. However, because of the increase of the number in possible one-wave multisoliton families themselves, the number of the corresponding bifurcated two-component branches also increases. For the even solitons considered in this work we have the following formula to calculate the number of two-wave subfamilies bifurcating from one-wave S_i family: $N_i=2^{(i+1)/2}$ (double that if we count the change signs of u and v). For example, there are 16 branches that bifurcate from S_7 branches that have $P=84$ at $\alpha=9$. Note that in the bifurcation diagram of Fig. 10, in order to clutter, only branches

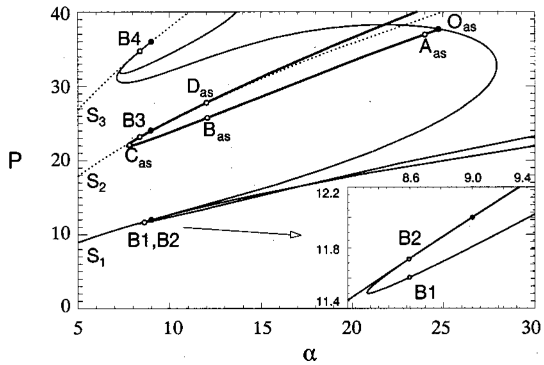

FIG. 17. Bifurcation diagram from the first three one-component families S_i, $i=1,2,3$. Asymmetric family S_2 is shown by a thick line.

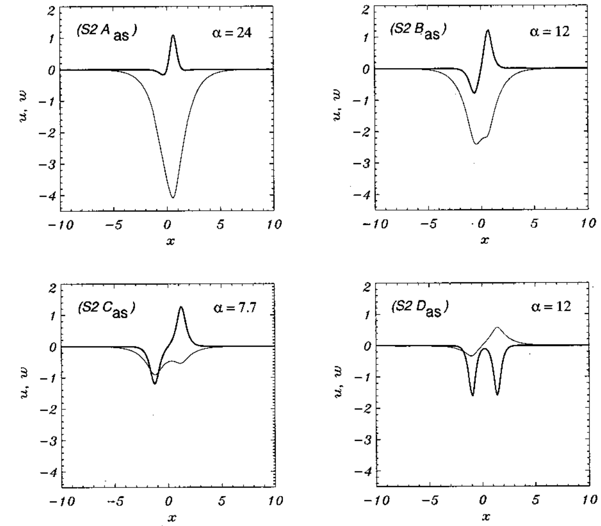

FIG. 19. Examples of asymmetric solutions bifurcated from the family S_2. Labeling of the profiles is in agreement with Fig. 17.

directly linked to the cascading limit two-wave family are shown. Close to bifurcation points, the third-harmonic components of the depicted branches have neighboring humps of alternating sign and first-harmonic components have all humps of the same sign. Note that these branches all bifurcate to the left of $\alpha=9$. For the branches that bifurcate to the right not all third harmonic neighboring humps alternate in sign.

It is important to note that none of the multihump soliton branches bifurcating to the left of $\alpha=9$ can be viewed as bound states of single partial solitons. Indeed, single one-hump solitons of Eqs. (1) *always* have u and w components inphase (of the same sign) for $\alpha<9.0$, whereas some of the individual humps of the of multihump structures bifurcating to the left from S_i $(i>1)$ families have u and w components of different signs. To illustrate this point we show in Fig. 17 an enlarged bifurcation diagram in the vicinity of $\alpha=9$ covering the first three families, S_i, $i=1,2,3$. Some of the corresponding examples of soliton profiles plotted at $\alpha=8.6$ are given in Fig. 18. As they approach $\alpha=9.0$, the separation between each individual hump (a ''partial soliton'') increases and the state begins to approach a concatenation of single solitons with slightly overlapping tails. However, some of these partial solitons have out-of-phase u and w components and hence *cannot exist* on their own (i.e., without being in superposition with other ''partial'' solitons).

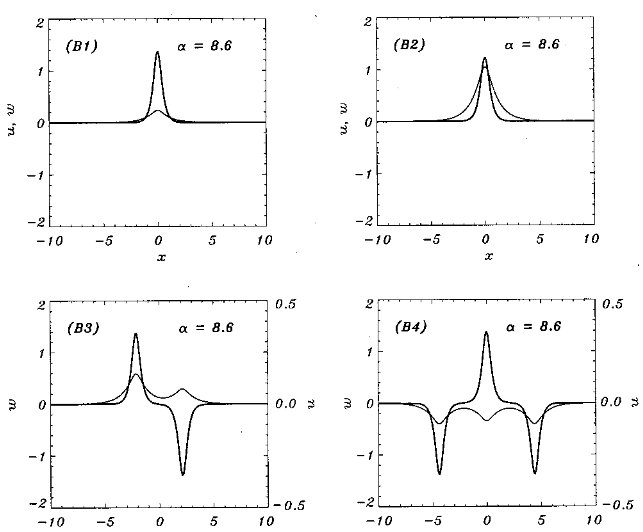

FIG. 18. Examples of the two-wave solitons close to bifurcation point at $\alpha=9$. Weak component $u(x)$ is enlarged in two bottom plots. Labeling of the profiles is in agreement with Fig. 17.

Figure 17 shows something even more striking—that there is also a ''bifurcation'' from the S_2 family. However, the solitary waves that bifurcate from there are not bright symmetric but in fact are *asymmetric* solitons, see Fig. 19. Also at least one of these asymmetric solutions is born in a symmetry-breaking (pitchfork) bifurcation from one of the symmetric soliton branches (at the point O_{as}, see Fig. 17). Thus there is a branch of asymmetric solitons that connects symmetric solitons with a branch of asymptotic antisymmetric solitons (the S_2 family). We conjecture that there are similar asymmetric solitons that ''bifurcate'' from S_j at $\alpha=9$ for all even j.

In contrast to the (2+1)D case, we have found no examples (at least considering all bifurcations from S_{2i+1} with $2i+1\leqslant 7$) of two-wave solitons that survive down to $\alpha=0$ where they might form a connection with branches of quasisolitons existing for $\alpha<0$. Instead, a representative branch coming from T_7 bends abruptly (at R) at which point α increases through the point S until it reaches T at $\alpha\approx 3.65$, where another nonlocal bifurcation occurs. In this process, the third harmonic gradually forms a core with weakly separated wings. At T, the latter become completely separated one-wave solitons [see Fig. 15(s,t)]. The solution at the point T can thus be viewed as a direct sum of two well-separated one-wave solitons and the soliton at point N. Beyond T we were unable to find any similar solutions. This nontrivial ''jump'' bifurcation is indicated by the vertical arrow in Fig. 10.

IV. CONCLUSION

In conclusion, we have investigated and classified higher-order soliton families and bifurcation phenomena due to resonant parametric interaction of a fundamental frequency wave with its third harmonic.

In the case of (2+1)D solitons the picture is consistent with standard theories, albeit the branch we followed from the cascading limit connects several distinct soliton types in a nontrivial way. Also the structure of the sets of branches we found to approach the limit $\alpha=0$ could do with further investigation, perhaps using singular perturbation theory. The relation of these states for positive α to quasisolitons for negative α will be addressed elsewhere.

In contrast, in the (1+1)D case the bifurcation diagram is less clear cut and we have found at least two features (i) the nonlocal bifurcation of multihumped two-frequency solutions that are a consequence of the local bifurcation from the one-humped one-frequency soliton at $\alpha=9$, and (ii) the so-called *jump* bifurcation at the point *T*. The first of these is particularly intriguing since not only symmetric multihumped states are formed in this way, but also asymmetric ones. The second novel bifurcation, the jump, appears related to, but not the same as, the so-called *orbit-flip* bifurcation [19]. A dynamical-systems-theory explanation of these new bifurcation events, perhaps using the Lin-Sandstede method as in Ref. [18], would be most interesting.

The conclusion that some of the discovered multihumped states cannot be viewed as bound states of several distinct one-humped states has significant physical implications. It demonstrates that a conventional approach to the construction of multihump solitons (see, e.g., [20]) gives only one possibility and that the parametric wave mixing may provide another, less straightforward way to create stationary higher-order modes. This may find application in many fields of physics where parametric interactions take place.

Stability of the newly discovered soliton families remains an open question, especially for the (1+1)D case. Although usually higher-order soliton families are subject to one of several types of instability, some exceptions are known (see, e.g., [21]) and thus a careful stability analysis is worth doing. For the conventional bound-state solitons of NLS-type system of equations, there is practically no hope of stability as shown e.g., in Ref. [22]. However, for the system under consideration there is a *real* possibility of detecting stable multihump solitons because of the abovementioned fact that at least some of them cannot be viewed as bound states of two or more single (one-hump) solitons.

ACKNOWLEDGMENTS

The authors acknowledge the use of computing facilities at Optical Sciences Centre, RSPhysSE, the Australian National University. A.V.B. and R.A.S. are indebted to O. Bang, L. Berge, B. A. Malomed, and D. Skryabin for useful discussions and interest in this work. A.R.C. is indebted for the hospitality of Yu. Kivshar at the RSPhysSE and to the UK EPSRC.

[1] S. Saltiel, S. Tanev, and A. D. Boardman, Opt. Lett. **22**, 148 (1997).
[2] R. A. Sammut, A. V. Buryak, and Yu. S. Kivshar, J. Opt. Soc. Am. B **15**, 1488 (1998).
[3] A. V. Buryak, V. V. Steblina, and R. A. Sammut, Opt. Lett. (to be published).
[4] D. L. Williams, D. P. West, and T. A. King, Opt. Commun. **148**, 208 (1998).
[5] D. E. Pelinovsky, V. V. Afanasjev, and Yu. S. Kivshar, Phys. Rev. E **53**, 1940 (1996).
[6] M. Haelterman, S. Trillo, and P. Ferro, Opt. Lett. **22**, 84 (1997).
[7] N. A. Ansari, R. A. Sammut, and H. T. Tran, J. Opt. Soc. Am. B **13**, 1419 (1996).
[8] A. R. Champneys and G. L. Lord, Physica D **102**, 101 (1996); V. E. Zakharov and E. A. Kuznetsov, Z. Éksp. Teor. Fiz. **113**, 1892 (1998) [JETP **86**, 1035 (1998)]; J. P. Boyd, *Weakly Nonlocal Solitary Waves and Beyond-All-Orders Asymptotics* (Kluwer, Dordrecht, 1998).
[9] A. V. Buryak, Phys. Rev. E **52**, 1156 (1995).
[10] E. Lombardi, Proc. R. Soc. Edinburgh, Sect. A: Math. **126**, 1035 (1996).
[11] A. V. Buryak and Y. S. Kivshar, Phys. Lett. A **197**, 407 (1995); A. D. Boardman, K. Xie, and A. Sengarpaul, Phys. Rev. A **52**, 4099 (1995); H. He, M. J. Werner, and P. D. Drummond, Phys. Rev. E **54**, 896 (1996); L. Torner and E. M. Wright, J. Opt. Soc. Am. B **13**, 864 (1996); A. Kobyakov, and F. Lederer, Phys. Rev. A **54**, 3455 (1996).
[12] N. G. Vakhitov and A. A. Kolokolov, Radiophys. Quantum Electron. **16**, 783 (1973); see also a review paper, E. A. Kuznetsov, A. M. Rubenchik, and V. E. Zakharov, Phys. Rep. **142**, 103 (1986).
[13] D. E. Pelenovsky, V. V. Afanasjev, and Yu. S. Kivshar, Phys. Rev. E **53**, 1940 (1996); O. Bang, Yu. S. Kivshar, A. V. Buryak, A. De Rossi, and S. Trillo, *ibid.* **58**, 5057 (1998).
[14] R. Y. Chiao, E. Garmire, and C. H. Townes, Phys. Rev. Lett. **13**, 479 (1964); **14**, 1056(E) (1965).
[15] K. Hayata, Y. Uehira, and M. Koshiba, Phys. Rev. A **51**, 1549 (1995).
[16] A. V. Buryak and N. N. Akhmediev, IEEE J. Quantum Electron. **31**, 682 (1995).
[17] A. C. Yew, A. R. Champneys, and P. J. McKenna, J. Nonlinear Sci. **9**, 33 (1999).
[18] A. C. Yew, B. Sandstede, and C. K. R. T. Jones, Phys. Rev. E **61**, 5886 (2000).
[19] B. Sandstede, C. K. R. T. Jones, and J. C. Alexander, Physica D **106**, 167 (1997).
[20] K. Klauder, E. W. Laedke, K. H. Spatschek, and S. K. Turitsyn, Phys. Rev. E **47**, R3844 (1993); A. V. Buryak, *ibid.* **52**, 1156 (1995); D. C. Calvo and T. R. Akylas, *ibid.* **56**, 4757 (1997).
[21] E. A. Ostrovskaya, Yu. S. Kivshar, D. V. Skryabin, and W. J. Firth, Phys. Rev. Lett. **83**, 296 (1999).
[22] A. V. Buryak and V. V. Steblina, J. Opt. Soc. Am. B **16**, 245 (1999); A. V. Buryak, Ph.D. thesis, Australian National University, 1996.